



The Modified Bidomain Model with Diffusive Inclusions

Yves Coudière, Andđela Davidović, Clair Poignard

► To cite this version:

Yves Coudière, Andđela Davidović, Clair Poignard. The Modified Bidomain Model with Diffusive Inclusions. Computing in Cardiology - 41st Annual Conference, Sep 2014, Cambridge, Massachusetts, United States. 2014. hal-01117258

HAL Id: hal-01117258

<https://inria.hal.science/hal-01117258>

Submitted on 16 Feb 2015

HAL is a multi-disciplinary open access archive for the deposit and dissemination of scientific research documents, whether they are published or not. The documents may come from teaching and research institutions in France or abroad, or from public or private research centers.

L'archive ouverte pluridisciplinaire **HAL**, est destinée au dépôt et à la diffusion de documents scientifiques de niveau recherche, publiés ou non, émanant des établissements d'enseignement et de recherche français ou étrangers, des laboratoires publics ou privés.

The Modified Bidomain Model with Diffusive Inclusions

Yves Coudière^{1,2,3,4}, Andjela Davidović^{1,2,3,4} (andjela.davidovic@inria.fr) and Clair Poignard^{1,2,3}

¹INRIA Bordeaux Sud-Ouest, ²University Bordeaux, ³Institut de Mathématiques de Bordeaux (IMB), ⁴IHU-Liryc

The standard bidomain model

- Widely accepted model
- Very good for the healthy tissues

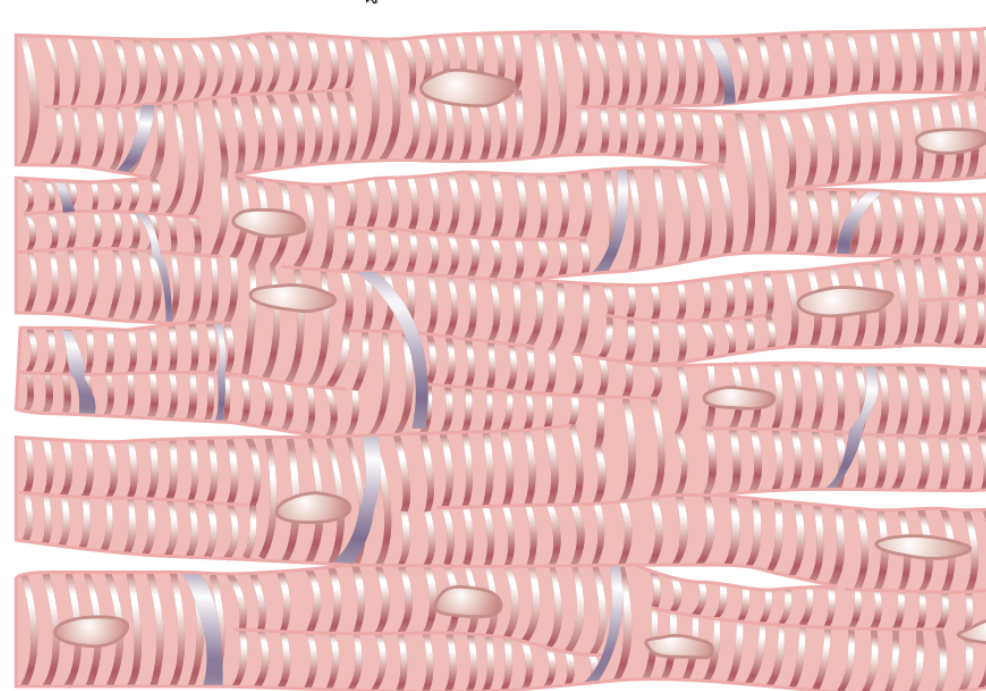


Figure: The patch of the cardiac tissue [4].

- Derived from the microscopic problem
- Assumptions used
 - periodicity
 - uniformly distributed ECM
 - anisotropic conductivities

Drawbacks - Examples

- There are non-small regions where myocytes are not present
- The laminar structure

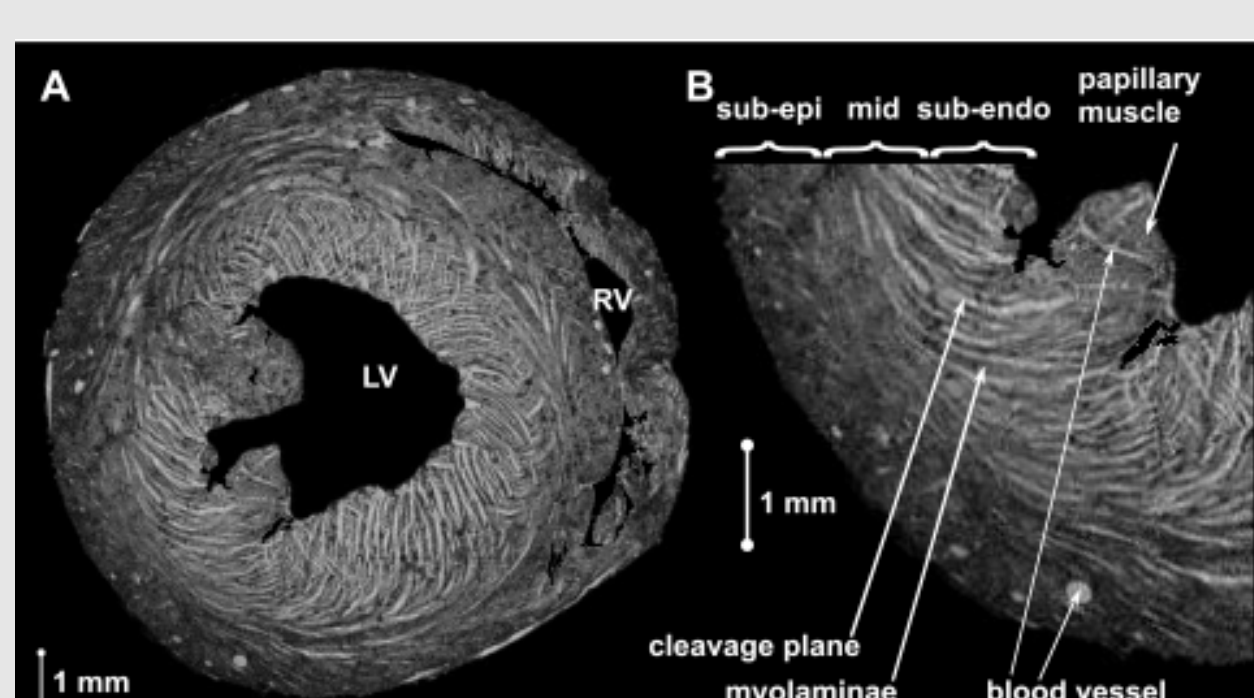


Figure: The laminar structure of myocardium. [2]

- The infarct border zone.

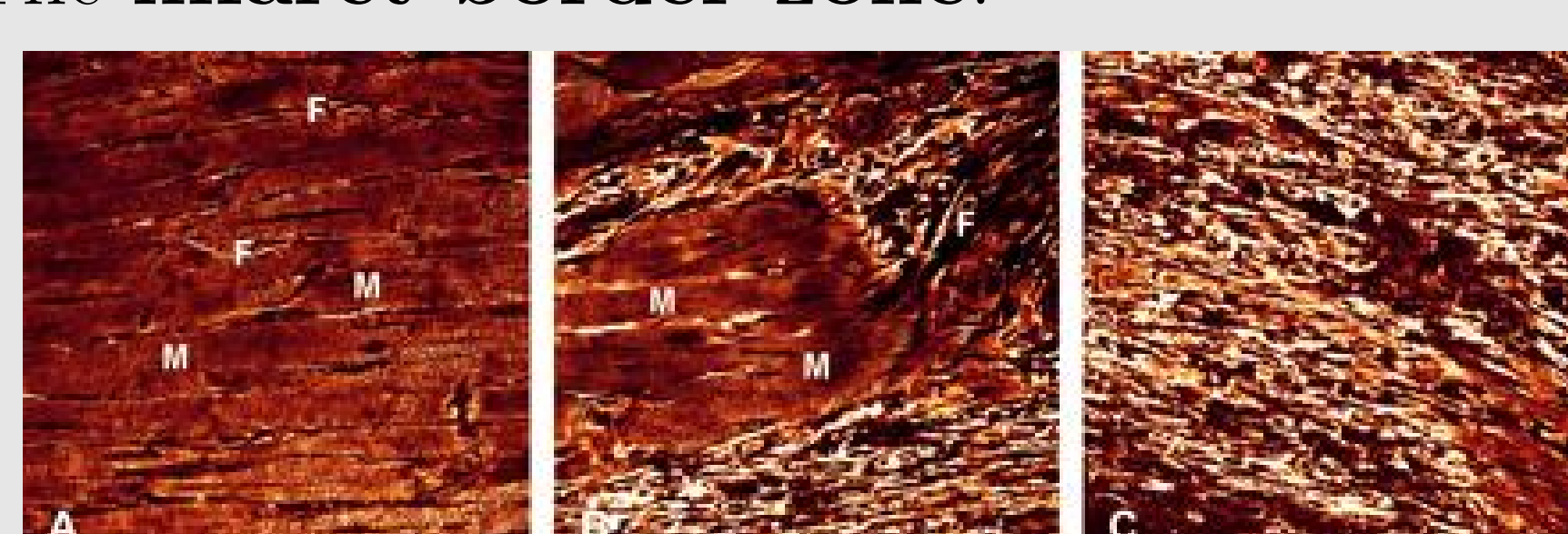


Figure: Fibroblast organization in sheep: normal ventricular myocardium (A), infarct border zone (B) and centre (C), 1 week after infarction. [3]

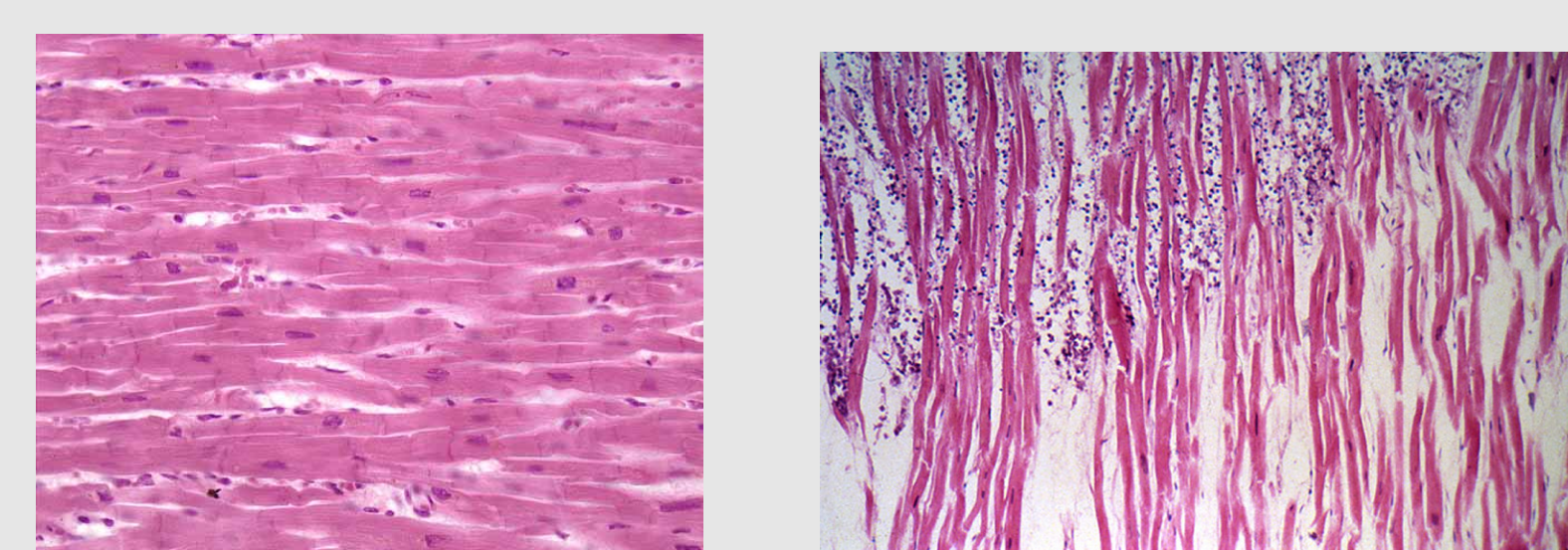
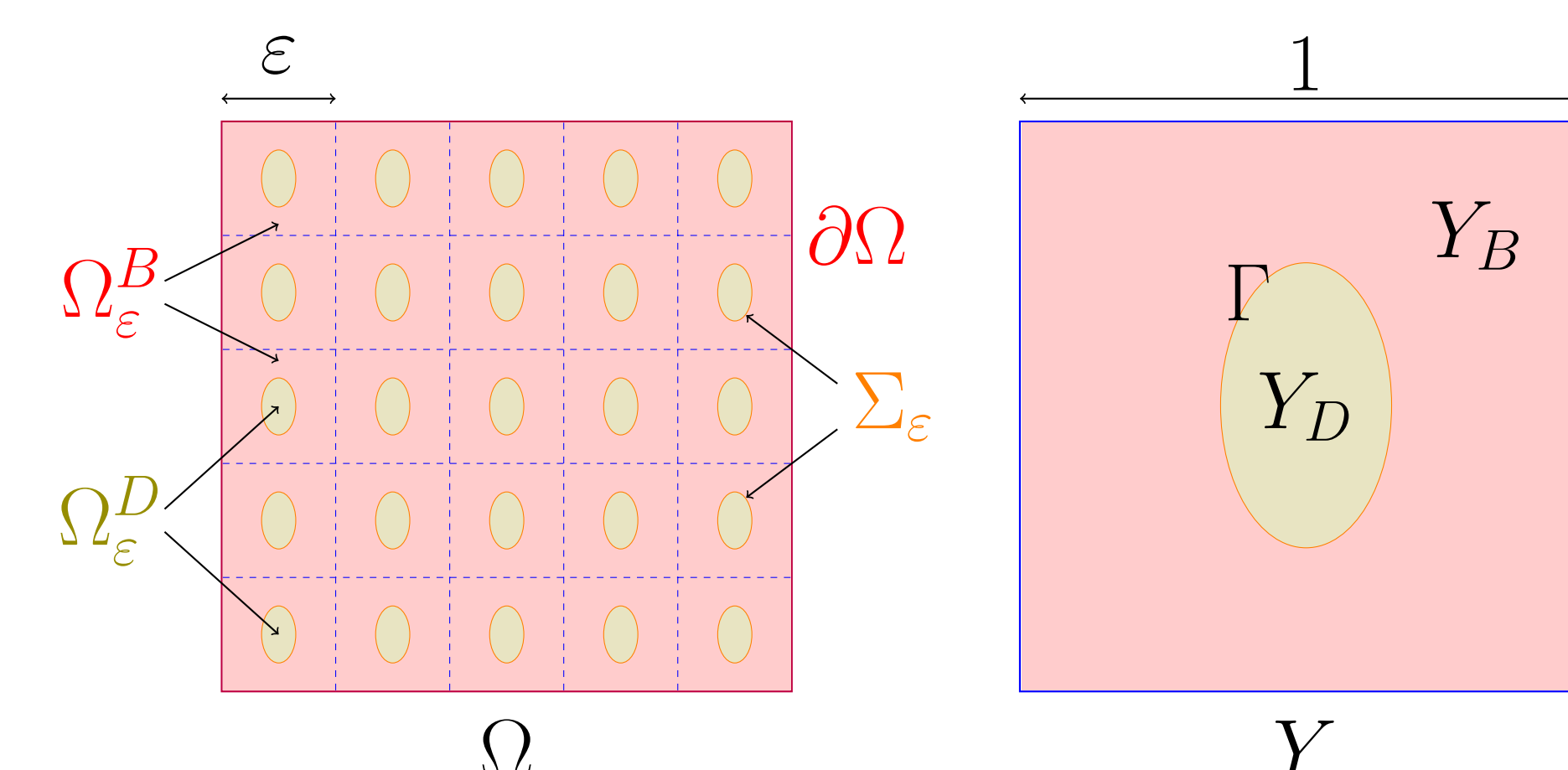


Figure: Normal tissue and Myocardial infarction in human. Tissue histology.

Modelling assumptions

- Periodic diffusive inclusions of size ε .
- Isotropic conductivity in the inclusions.
- No cells in the inclusions. Passive conductors.
- Standard transmission conditions.

Microscale model



Bidomain model

$$\begin{aligned} \partial_t h_\varepsilon + g(v_\varepsilon, h_\varepsilon) &= 0, & \text{in } \Omega_\varepsilon^B, \\ \partial_t v_\varepsilon + I_{ion}(v_\varepsilon, h_\varepsilon) &= \nabla \cdot (\sigma_\varepsilon^i \nabla u_\varepsilon^i), & \text{in } \Omega_\varepsilon^B, \\ \partial_t v_\varepsilon + I_{ion}(v_\varepsilon, h_\varepsilon) &= -\nabla \cdot (\sigma_\varepsilon^e \nabla u_\varepsilon^e), & \text{in } \Omega_\varepsilon^B. \end{aligned}$$

- intra- and extra-cellular conductivities σ_ε^i and σ_ε^e
- unknown potentials u_ε^i and u_ε^e
- transmembrane potential $v_\varepsilon := u_\varepsilon^i - u_\varepsilon^e$
- $I_{ion}(v, h)$ and $g(v, h)$ define specific ionic model

Diffusive inclusions

$$\nabla \cdot (\sigma_\varepsilon^d \nabla u_\varepsilon^d) = 0, \quad \text{in } \Omega_\varepsilon^D.$$

- conductivity σ_ε^d
- unknown potential u_ε^d

Interface

$$\left. \begin{aligned} \sigma_\varepsilon^i \nabla u_\varepsilon^i \cdot \mathbf{n}_{\Sigma_\varepsilon} &= 0, \\ \sigma_\varepsilon^e \nabla u_\varepsilon^e \cdot \mathbf{n}_{\Sigma_\varepsilon} &= \sigma_\varepsilon^d \nabla u_\varepsilon^d \cdot \mathbf{n}_{\Sigma_\varepsilon}, \\ u_\varepsilon^e &= u_\varepsilon^d, \end{aligned} \right\} \quad \text{on } \Sigma_\varepsilon.$$

Method: Homogenisation

Assume:

$$\begin{aligned} u_\varepsilon^i(t, x) &= u_0^i(t, x) + u_1^i(t, x, \frac{x}{\varepsilon}) + \dots, \\ u_\varepsilon^e(t, x) &= u_0^e(t, x) + u_1^e(t, x, \frac{x}{\varepsilon}) + \dots. \end{aligned}$$

- Let $\varepsilon \rightarrow 0$. Derive the homogenised problem and the cell problems.
- According to [1], *a priori* estimates ensure the two-scale convergence

Limit macroscale model

- The limit problem in whole Ω :

$$\begin{aligned} \partial_t h_0 + g(v_0, h_0) &= 0, \\ |Y_B|(\partial_t v_0 + I_{ion}(v_0, h_0)) &= \nabla \cdot (\tilde{\sigma}_i \nabla u_0^i), \\ |Y_D|(\partial_t v_0 + I_{ion}(v_0, h_0)) &= -\nabla \cdot (\tilde{\sigma}_e \nabla u_0^e). \end{aligned}$$

- New conductivities

$$\begin{aligned} \tilde{\sigma}_i &= \sigma^i |Y_B| + A^i(\sigma_i, w^i), \\ \tilde{\sigma}_e &= \sigma^e |Y_B| + \sigma^d |Y_D| + A(\sigma_e, \sigma_d, w) \end{aligned}$$

where A_i and A are matrices obtained by solving the cell problems on Y for unknown functions w^i and w .

Remarks:

- The conductivities depend on the volume fraction and on the geometry of the diffusive part.
- If $\sigma_e = \sigma_d$ then on the volume fraction only.
- If $|Y_D| = 0$ it is the standard bidomain model.
- If $|Y_B| = 0$ it is only the diffusion model.

Numerical results

- *FreeFem++* and *gnuplot*.
- Mitchell Schaeffer ionic model.
- 2D simulations on Ω rectangle, SBDF2 numerical scheme.
- Simple shapes of inclusions (circles and ellipses).

Table: The values of the new conductivities depending on the diffusion inclusions [10^{-1}S/m]. The first row: values for the standard bidomain model, without inclusions.

geometry	vol frac	σ^d	σ_{i11}^*	σ_{i22}^*	σ_{e11}^*	σ_{e22}^*
-	-	-	1.74	0.19	3.9	1.97
circle	0.18	3	1.29	0.18	3.28	2.45
ellipse (1:4)	0.18	3	0.31	0.19	0.75	2.61
circle	0.2	3	1.26	0.17	3.29	2.53
ellipse (1:1.5)	0.2	3	1.13	0.18	2.82	2.58
ellipse (1:2)	0.2	3	0.86	0.18	2.09	2.64
circle	0.4	3	1.07	0.15	3.42	3.53
ellipse (1:1.5)	0.4	3	0.81	0.16	2.53	3.70
circle	0.7	3	0.69	0.09	5.08	7.89

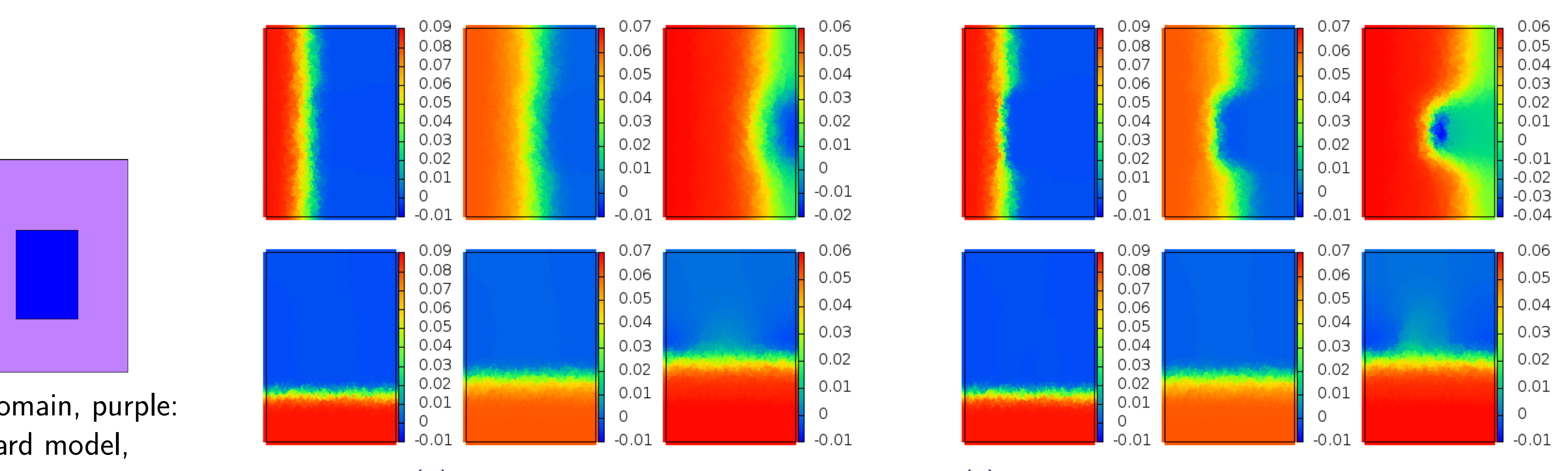


Figure: Simulation of the standard bidomain with the "scar patch". $\sigma^d = 3$, volume fraction 0.18, comparing inclusions geometries.

Conclusions

- Inclusions change the speed of propagation and depending on geometry, the anisotropy ratio.
- Rigorous and practical way to link the structural disease to macroscopic conductivities.

Future work

- Use the late enhancement MRI for the volume fraction of the extracellular space.
- Cells in the additional ECM. Boundary conditions.

References

- [1] Allaire, Gregoire. "Homogenization and two-scale convergence." SIAM Journal on Mathematical Analysis 23.6 (1992): 1482-1518.
- [2] Gilbert, Stephen H., et al. "Visualization and quantification of whole rat heart laminar structure using high-spatial resolution contrast-enhanced MRI." American Journal of Physiology-Heart and Circulatory Physiology 302.1 (2012): H287-H298.
- [3] Camelliti, Patrizia, Thomas K. Borg, and Peter Kohl. "Structural and functional characterisation of cardiac fibroblasts." Cardiovascular research 65.1 (2005): 40-51.
- [4] Hall, John E. Guyton and Hall Textbook of Medical Physiology: Enhanced E-book. Elsevier Health Sciences, 2010.